JOURNAL OF PROPULSION AND POWER
Vol. 26, No. 3, May–June 2010

Acoustic Analysis of Hybrid Rocket Combustion Chambers

Dario Pastrone,* Lorenzo Casalino,* and Matteo Rosa Sentinella†
Politecnico di Torino, Turin 10129, Italy
and
Carmine Carmicino‡
University of Naples "Federico II," Naples 80125, Italy

DOI: 10.2514/1.39578

A method based on passive linear stability measurement has been developed to investigate combustion dynamics in hybrid rocket motors. A one-dimensional model is used to describe the acoustic motions inside the rocket chamber as a function of the motor axial coordinate. The equations of mass, momentum, and energy are solved for the average flow. A linearized analysis, which takes combustion response functions into account, provides pressure and velocity acoustic oscillations. When the boundary conditions at the nozzle inlet are enforced and the response functions are known, the acoustic modes and growth constant can be derived, whereas the coupled responses can be determined from the experimental measurement of the mode frequencies. If noise sources in the control volume are accounted for, then it is theoretically possible to determine the response functions at all frequencies simply by measuring the pressure fluctuations at the head end of the motor. Experimental data are analyzed and contrasted to the proposed one-dimensional model, showing a good agreement.

Nomenclature

A	=	port area
A_{SN}	=	short-nozzle admittance
a	=	sound speed
B	=	matrix of coefficients, Eq. (17)
C	=	vector of coefficients, Eq. (18)
C_p	=	constant pressure specific heat
C_v	=	constant volume specific heat
D	=	vector of coefficients, Eq. (20)
E	=	matrix of coefficients, Eq. (22)
e	=	specific internal energy
f	=	frequency
h_b	=	fuel heating value
i	=	imaginary unit
M	=	Mach number
M_i	=	nozzle inlet Mach number
$\dot{m}_b$	=	fuel mass flow rate per unit length
$\mathcal{P}$	=	burning surface perimeter
p	=	pressure
Q	=	matrix of coefficients, Eq. (16)
R	=	gas constant
R_p	=	regression rate pressure-coupled response
R_v	=	regression rate velocity-coupled response
T	=	temperature
t	=	time
u	=	velocity
u_b	=	mass injection velocity
x	=	chamber axial abscissa
α	=	growth constant
β	=	coefficient
γ	=	specific heat ratio
γ_s	=	isentropic exponent
ν	=	noise level
ρ	=	density
ρ_b	=	solid fuel density
ω	=	angular frequency

Superscripts

$'$	=	fluctuation
$\hat{}$	=	fluctuation wave shape
$\bar{}$	=	average

Presented as Paper 5368 at the 43th AIAA/ASME/SAE/ASEE Joint Propulsion Conference and Exhibit, Cincinnati, OH, 8–11 July 2007; received 8 July 2008; accepted for publication 28 December 2009.

*Associate Professor, Dipartimento di Energetica, Corso Duca degli Abruzzi, 24. Senior Member AIAA.

†Research Assistant, Dipartimento di Energetica, Corso Duca degli Abruzzi, 24.

‡Research Consultant, Dipartimento di Ingegneria Aerospaziale, P.le Tecchio 80; currently at General Electric Oil & Gas, Via Felice Matteucci 2, Florence, Italy. Member AIAA.

I. Introduction

HYBRID rocket motors display a more stable combustion behavior when compared to solid or liquid propellant rockets. Based on past experience, catastrophic instabilities are not expected to occur, but requirements related to mission, attitude control, payload, and vehicle structure limit the allowable thrust oscillations; a better understanding of combustion process and related instability is therefore desirable. Recent studies seem to be mainly devoted to low-frequency instability, because this is the most common combustion instability that has been experienced during firing tests [1], in the form of limit cycle oscillations. Low-frequency instability has been verified to be usually accompanied by the excitation of longitudinal acoustic modes. In particular, acoustic modes are driven if a radial injector is employed, whereas an axial one has provided stable combustion in all the experimental tests [2]. Also, techniques have been developed that use Helmholtz oscillations to determine ballistic parameters such as the regression rate of the fuel grain [3]. In this context, improved techniques that allow for an accurate prediction and minimization of high-frequency pressure oscillations inside the combustion chamber of hybrid rockets have been sought; they could also be used to improve the knowledge of the combustion process.

Combustion instability of solid and liquid systems has been studied extensively, and many investigation methods have been proposed and applied. One of these methods is the passive linear stability measurement (PLSM), proposed by Hessler [4], which, according to Culick [5], corresponds to system identification. This experimental method, which was the subject of considerable work and discussion in the past, would allow for the determination of the stability margin of a solid rocket motor without introducing external

disturbances. The PLSM method is based on the fact that, due to the presence of forcing terms, small pressure oscillations exist at any mode frequency, although the mode considered is a stable one. These pressure oscillations are either damped or amplified, depending on the acoustic characteristics of the particular mode considered and the coupling between the acoustics of the combustion chamber and the forcing terms. The relation between the acoustic properties of the chamber, the forcing functions, and the acoustic energy gain/loss mechanisms can be expressed in terms of coupling integrals. Thus, two different approaches to the problem can be envisaged. If the coupling integrals, the energy gain/loss mechanism, and the forcing functions are known, either theoretically or from experimental measurements, it is possible to predict the behavior of the pressure oscillation inside the rocket motor. On the other hand, it is in principle possible to determine the forcing functions and the gain/loss mechanisms of acoustic energy by measuring the pressure oscillations inside the chamber during normal operation of a rocket motor and from the knowledge of the coupling integrals. The described methodology has been successfully applied to the instability analysis of solid rocket motors [6–8].

In the present article, this approach is extended to analyze the combustion process in hybrid rocket motors. Conservation equations are rewritten to take into account the different combustion mechanisms with respect to solid propellant rocket motors. Specifically, gas temperature and gas property variations along the grain axis are taken into account. Then, with appropriate boundary conditions, these equations are solved to determine the pressure fluctuations anywhere along the chamber. The knowledge of the pressure fluctuations from experimental measurements allows for the investigation of the combustion process; experimental data have been analyzed and contrasted to the results obtained using the proposed model. Results show that the approaches classically used to analyze solid rocket motor combustion can be profitably applied in the case of hybrid rocket motors.

II. Experimental Results

A brief description of the lab-scaled hybrid motor, test facility, and data reduction technique is reported along with some experimental results; more details can be found in [2,9]. A scheme of the motor is shown in Fig. 1. Gaseous oxygen can be supplied by a reservoir of eight cylinders at mass flow rates up to 0.3 kg/s. The oxygen mass flow rate is derived by measuring the gas temperature (with a copper–constantan thermocouple) and pressure at a section upstream of the throat of a home-designed sonic venturi tube. Installing this device was mandatory to isolate the combustion chamber dynamics from the rocket feed system, thus allowing us to consider the oxidizer mass flow as constant, that is, independent of the pressure oscillations in the combustion chamber. The combustion chamber is axisymmetric; it is 720 mm long and has a 133 mm inner case diameter. Single port fuel grains of high-density polyethylene (HDPE) or hydroxyl-terminated polybutadiene were tested on the motor in a configuration with either an axial or a radial injector [10,11]. In both cases, two chambers were set up ahead and aft of the fuel grain; the precombustion chamber is 65 mm long with an 80 mm diameter. When coupled with the axial injector, it serves to shift toward the fore end of the grain the strong recirculation region caused by the oxygen injection, thus increasing the overall regression rate. When used with the radial injector assembly, the prechamber instead serves as a dump plenum. The aft-mixing chamber (75 mm long with a 90 mm diameter) promotes further gas mixing at the exit of the fuel grain, thereby improving the combustion efficiency. A water-cooled converging–diverging nozzle with a 16 mm throat diameter, 2.44 area ratio, made of a copper alloy ensures long duration firings with no throat erosion. Motor ignition was accomplished using an electrically driven pyrotechnic cartridge.

Low-frequency chamber pressure was measured by two capacitive transducers, Setra model 280E, set up in the prechamber and in the aft-mixing chamber. On the other hand, high-frequency pressure oscillations were obtained in the dump plenum using a PCB® helium bleed dynamic pressure gauge model 123 A, flush mounted on the motor forward closure (see Fig. 1). The analog signals coming from all the sensors were sampled at 10 kHz, digitally converted (16-bit resolution), processed, and recorded by a National Instruments (NI) SCXI system interconnected with a PC via an NI 6034 E PCI data acquisition card. With this equipment and by using a dedicated software developed in LabView 7, the motor is ignited and the firing test is completely automated. All the signals are saved in a binary format for postprocessing and, after down-sampling to 100 Hz (by averaging the data), in text format. To remove the power line interference at 50 Hz and its higher harmonics from the high-frequency pressure data output by the PCB transducer, the fast Fourier transform (FFT) of the data was performed; in doing that the data were symmetrically zero padded to the next power of two and windowed through a Hanning window with the purpose of minimizing the spectral leakage. The points of the amplitude spectrum at the power line interference harmonics were substituted with an average of the nearby points in the spectrum; then, the inverse FFT was computed to give back the filtered signal in the time domain. Then, pressure signals were bandpass filtered using a 1–4500 Hz passband with the twofold aim of taking apart the slow varying average pressure from the high-frequency signals and of eliminating aliasing. Phase shift resulting from this filtering process was removed as follows: the signal was first filtered with increasing time and then filtered back from the last point with decreasing time [12]. The resulting data were analyzed with the short-time Fourier transform (STFT) technique to map the oscillation amplitude over the joint frequency-time domain. We recall that the STFT of the generic signal $x(t)$ is defined by the following relationship [13]:

$$\mathrm{STFT}\,(t_0, f) = \int_{-\infty}^{+\infty} x(t)w(t - t_0)e^{-i2\pi ft}\,\mathrm{d}t \tag{1}$$

where $w(t)$ is commonly referred to as a window function. STFT is, then, a function of the frequency f and of the time instant t_0, where the window function is centered, and represents the Fourier transform of the given signal around t_0. The data were transformed using a Gaussian window of a 2 s period and a time increment of 1 s, resulting in 50% overlapped data, to give the spectrogram, that is, the squared magnitude of the STFT.

Figure 2 shows the pressure spectrogram, normalized with respect to the corresponding maximum amplitude, for the gaseous oxygen and HDPE propellant combination. It is seen that the pressure fluctuation spectrum exhibits a peak around 450 Hz, which corresponds to the first longitudinal mode of the chamber. Additional peaks are present at higher frequencies. As expected in the case of an

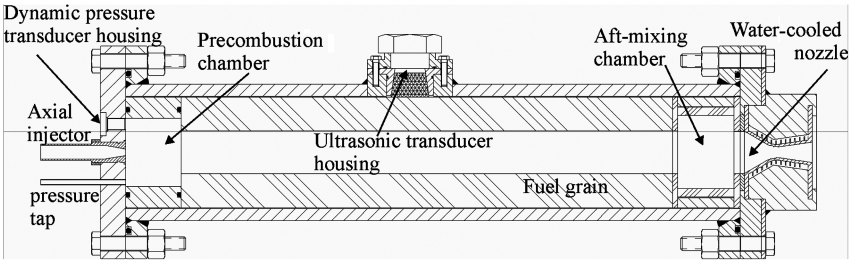

Fig. 1 Scheme of the lab-scaled hybrid motor.

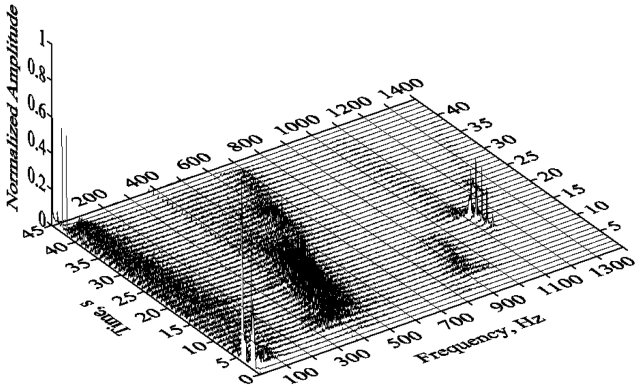

Fig. 2 Normalized spectrogram of the head-end pressure.

acoustic enclosure in which stochastic noise sources are present, the pressure power spectrum is composed of several broad peaks centered around the modal frequencies of the combustion chamber.

III. One-Dimensional Model

The one-dimensional model presented in a previous paper [8] is here extended to deal with the peculiarities of the combustion of hybrid propellants. The governing equations for one-dimensional longitudinal waves were obtained starting from the conservation equations of mass, momentum, and energy written for a constant cross-sectional cylindrical chamber with mass injection from the walls:

$$\frac{\partial \rho}{\partial t} + \frac{\partial \rho u}{\partial x} = \frac{\dot{m}_b}{A}\left(1 - \frac{\rho}{\rho_b}\right) \tag{2}$$

$$\rho \frac{\partial u}{\partial t} + \rho u \frac{\partial u}{\partial x} + \frac{\partial p}{\partial x} = -u \frac{\dot{m}_b}{A}\left(1 - \frac{\rho}{\rho_b}\right) \tag{3}$$

$$\rho \frac{\partial e}{\partial t} + \rho u \frac{\partial e}{\partial x} = \frac{\dot{m}_b}{A}\left[h_b + \frac{u_b^2}{2} - \left(e - \frac{u^2}{2}\right)\left(1 - \frac{\rho}{\rho_b}\right)\right] - p \frac{\partial u}{\partial x} \tag{4}$$

The present formulation introduces some differences with respect to models classically used for unsteady motions in solid rocket motors. For the sake of simplicity, the combustion process in the port is modeled by considering the heating of a perfect gas ($p = \rho RT$). The variation of the gas composition along the grain axis is taken into account. The mean specific heat $C_v = e/T$ is introduced and both C_v and T vary along the grain length. Also, the energy addition from the propellant combustion is represented by $\dot{m}_b(h_b + u_b^2/2)$.

Under the assumption that gas density is much lower than the solid fuel density, $1 - \rho/\rho_b \approx 1$. The energy equation is multiplied by R/C_v, the continuity equation by RT, and the resulting equations are added to obtain an equation for pressure and velocity:

$$\frac{\partial p}{\partial t} + u \frac{\partial p}{\partial x} + \frac{C_p}{C_v} p \frac{\partial u}{\partial x} = \frac{R}{C_v}\frac{\dot{m}_b}{A}\left(h_b + \frac{u_b^2}{2} + \frac{u^2}{2}\right) - p\left(\frac{1}{C_v}\frac{\partial C_v}{\partial t} - \frac{1}{R}\frac{\partial R}{\partial t}\right) - up\left(\frac{1}{C_v}\frac{\partial C_v}{\partial x} - \frac{1}{R}\frac{\partial R}{\partial x}\right) \tag{5}$$

A linear approach is adopted and each variable (except the gas thermodynamic properties, which are assumed to be constant with respect to time) is written as the sum of a time-averaged part plus a fluctuation, which is assumed to be small compared to the average quantities. For the average solution, the time derivatives are small and can be neglected compared to the axial derivatives; therefore,

$$\rho u^2 \frac{\partial u}{\partial x} + u^3 \frac{\partial \rho}{\partial x} = \frac{\dot{m}_b}{A} u^2 \tag{6}$$

$$\rho u^2 \frac{\partial u}{\partial x} + u \frac{\partial p}{\partial x} = -\frac{\dot{m}_b}{A} u^2 \tag{7}$$

$$\frac{C_p}{C_v} p \frac{\partial u}{\partial x} + u \frac{\partial p}{\partial x} = \frac{R}{C_v}\frac{\dot{m}_b}{A}\left(h_b + \frac{u_b^2}{2} + \frac{u^2}{2}\right) + \frac{upC_v}{R}\frac{\partial C_p/C_v}{\partial x} \tag{8}$$

which are further elaborated to obtain the derivative of the state variables u, p, and ρ explicitly:

$$\gamma p(1 - M^2)\frac{\partial u}{\partial x} = (\gamma - 1)\frac{\dot{m}_b}{A}\left(h_b + \frac{u_b^2}{2}\right) + (\gamma + 1)\frac{\dot{m}_b}{A}\frac{u^2}{2} + \frac{up}{(\gamma - 1)}\frac{\partial \gamma}{\partial x} \tag{9}$$

$$u(M^2 - 1)\frac{\partial p}{\partial x} = (\gamma - 1)M^2 \frac{\dot{m}_b}{A}\left(h_b + \frac{u_b^2}{2} + \frac{u^2}{2}\right) + \frac{\dot{m}_b}{A}u^2 + M^2 \frac{up}{(\gamma - 1)}\frac{\partial \gamma}{\partial x} \tag{10}$$

$$u^2 \frac{\partial \rho}{\partial x} = 2\frac{\dot{m}_b}{A}u + \frac{\partial p}{\partial x} \tag{11}$$

where the ratio of the specific heats $\gamma = C_p/C_v = (C_v + R)/C_v$ and the Mach number $M = u/\sqrt{\gamma p/\rho}$, which is defined using γ instead of the correct isentropic exponent γ_s, have been introduced to simplify the notation. The varying gas temperature and properties (molecular mass, gas constant, specific heat at constant pressure, and isentropic exponent) are known in the prechamber and in the aft-mixing chamber. A linear approximation is assumed to describe the variation of R, γ, and γ_s along the grain axis. Constant energy addition along the grain length is also assumed, and the proper constant value of h_b is determined a posteriori to have the expected temperature at the grain exit.

By linearizing the equations and subtracting the conservation equation for average quantities, the following equations for pressure and velocity fluctuations are obtained:

$$\bar{\rho}\frac{\partial u'}{\partial t} + \frac{\partial p'}{\partial x} = -\rho' \bar{u}\frac{\partial \bar{u}}{\partial x} - \bar{\rho}\frac{\partial \bar{u}u'}{\partial x} - \frac{u'\overline{\dot{m}}_b}{A} - \frac{\dot{m}'_b \bar{u}}{A} \tag{12}$$

$$\frac{\partial p'}{\partial t} + \bar{u}\frac{\partial p'}{\partial x} + \gamma \bar{p}\frac{\partial u'}{\partial x} = -u'\frac{\partial \bar{p}}{\partial x} - \gamma p'\frac{\partial \bar{u}}{\partial x} + \frac{(\gamma - 1)}{A}\left[\dot{m}'_b\left(h_b + \frac{\bar{u}_b^2}{2} + \frac{\bar{u}^2}{2}\right) + \overline{\dot{m}}_b(\bar{u}_b u'_b + \bar{u}u')\right] \tag{13}$$

It is assumed that the separation of variables can be applied so that pressure, velocity, and injected mass fluctuations can be written as

$$p' = \hat{p}(x)e^{i\omega t}; \qquad u' = \hat{u}(x)e^{i\omega t}; \qquad \dot{m}'_b = \widehat{\dot{m}}_b(x)e^{i\omega t} \tag{14}$$

where, in general, ω is a complex number. By substituting these definitions into the preceding equations, assuming that the pressure fluctuations are isentropic, that is,

$$\rho' = \frac{p'}{a^2} = \frac{p'}{\gamma_s \bar{p}/\bar{p}}$$

and considering that

$$u'_b = \frac{\dot{m}'_b}{\bar{\rho}\bar{\mathcal{P}}} - \frac{\rho'}{\bar{\rho}}\bar{u}_b$$

the following equations for the variables $\hat{p}(x)$ and $\hat{u}(x)$ are obtained:

$$Q(x)\frac{\mathrm{d}}{\mathrm{d}x}\begin{bmatrix}\hat{u}\\ \hat{p}\end{bmatrix} + B(x)\begin{bmatrix}\hat{u}\\ \hat{p}\end{bmatrix} = C(x)\widehat{\dot{m}}_b \tag{15}$$

where the coefficient matrices $Q(x)$, $B(x)$, and $C(x)$ have the following form:

$$Q(x) = \begin{bmatrix} \overline{\rho u} & 1 \\ \gamma \bar{p} & \bar{u} \end{bmatrix} \tag{16}$$

$$B(x) = \begin{bmatrix} \bar{\rho}\frac{\partial \bar{u}}{\partial x} + \frac{\overline{\dot{m}}_b}{A} + i\omega\bar{\rho} & \frac{\bar{u}}{a^2}\frac{\partial \bar{u}}{\partial x} \\ \frac{\partial \bar{p}}{\partial x} - \frac{\gamma-1}{A}\overline{\dot{m}}_b\bar{u} & \gamma\frac{\partial \bar{u}}{\partial x} + \frac{\gamma-1}{A}\frac{\overline{\dot{m}}_b\bar{u}_b^2}{\bar{\rho}a^2} + i\omega \end{bmatrix} \tag{17}$$

$$C(x) = \begin{bmatrix} -\frac{\bar{u}}{A} \\ \frac{\gamma-1}{A}\left[(h_b + \frac{\bar{u}_b^2}{2} + \frac{\bar{u}^2}{2}) + \frac{\overline{\dot{m}}_b\bar{u}_b}{\bar{\rho}\bar{p}}\right] \end{bmatrix} \tag{18}$$

Fuel mass flow rate oscillations are supposed to be linearly related to $\hat{u}$ and $\hat{p}$:

$$\hat{\dot{m}}_b = D^T(x)\begin{bmatrix} \hat{u} \\ \hat{p} \end{bmatrix} \tag{19}$$

where, in analogy with the case of solid propellant, pressure- and velocity-coupled response functions are introduced assuming their effects to be additive [14,15]:

$$D(x) = \overline{\dot{m}}_b\begin{bmatrix} R_v/a \\ R_p/\bar{p} \end{bmatrix} \tag{20}$$

Alternative formulations have also been proposed [16], in particular to analyze nonlinear instability; these approaches are not considered here.

With respect to the solid propellant case, the main difference is that these response functions are not only related to the propellant itself, but also to the peculiar hybrid combustion process in the boundary layer. Equation (15) can be rewritten as

$$\frac{\mathrm{d}}{\mathrm{d}x}\begin{bmatrix} \hat{u} \\ \hat{p} \end{bmatrix} + E(x)\begin{bmatrix} \hat{u} \\ \hat{p} \end{bmatrix} = 0 \tag{21}$$

with

$$E(x) = Q^{-1}(x)B(x) - Q^{-1}(x)C(x)D^T(x) \tag{22}$$

These equations cannot be solved analytically and are numerically integrated once the proper boundary conditions are imposed.

The motor is composed of three constant cross-sectional elements and the nozzle. The average variables equations can be solved for each part of the motor separately; in particular, Eqs. (9–11) show that the average quantities are constant in the prechamber and mixing chamber, because $\dot{m}_b$ is null. The interaction between the different motor parts is accounted for by enforcing appropriate boundary conditions at the junction between two adjacent elements. The impedance at the jth area change is neglected and only the mass and energy conservation are taken into account to relate the quantities after the discontinuity (subscript $j+$) to those before (subscript $j-$):

$$\begin{aligned} p_{j+} &= p_{j-} \qquad \rho_{j+}u_{j+}A_{j+} = \rho_{j-}u_{j-}A_{j-} \\ T_{j+} + u_{j+}^2/(2C_p) &= T_{j-} + u_{j-}^2/(2C_p) \qquad j = 1, 2 \end{aligned} \tag{23}$$

Boundary conditions at the motor head end and at the nozzle inlet section must also be given. At the motor head end, a zero acoustic velocity is enforced. The impedance of the nozzle can be estimated by assuming that the short choked nozzle approximation holds true. In this approximation the nozzle has only a damping effect on the acoustic oscillations inside the chamber, that is, the imaginary part of the nozzle impedance is equal to zero. The magnitude of the damping provided by the nozzle is a function of the flow Mach number at the inlet of the nozzle and is given by

$$A_{\mathrm{SN}} = \frac{u'}{a}\frac{\gamma\bar{p}}{p'} = M_i\frac{\gamma_s - 1}{2}$$

where the actual Mach number $M = u/\sqrt{\gamma_s R\bar{T}}$ appears. In certain cases, this impedance may be not sufficiently rigorous to accurately predict mode frequencies and mode shapes of a combustion chamber [17]. In these cases, a fully three-dimensional analysis of the acoustic motions inside the nozzle is necessary to evaluate the nozzle impedance.

IV. Parametric Study

The knowledge of the average quantities and their derivatives, along with the values of the regression rate, combustion gas properties, and velocity and pressure-coupled response functions is needed to solve the system of equations represented by Eq. (21). Average pressure, velocity, and density and their derivatives with respect to the axial coordinate are calculated according to Eqs. (9–11). Test case 1-A in [9] has been selected as a reference case; 0.11 kg/s of oxygen enter the prechamber at 300 K. The analysis has been conducted 15 s after ignition, when the port area is $A = 17$ cm^2, the space-averaged regression rate is estimated to be 0.535 mm/s, according to the procedure reported in [18], and the mean mixture ratio is 2.37. The gas stagnation temperature at the nozzle inlet is 3555 K.

A parametric study was performed by changing the real and/or imaginary part of each of the response functions while maintaining the other fixed. If the boundary condition imposed by the nozzle is not taken into account, and the real and imaginary parts of ω are assigned, a simple forward integration of the equations, starting from the head end, yields pressure and velocity wave amplitudes as a function of the axial coordinate x. Figure 3 is an example of the results obtained during this parametric study, assuming a real frequency $f = 1000$ Hz, close to the second longitudinal mode, that is, $\mathrm{Re}(\omega) = 2\pi f$ and $\mathrm{Im}(\omega) = 0$. In agreement with results obtained by other authors [14] in the case of solid rocket motors, the shape of pressure waves is affected by the imaginary part of R_p and the real part of R_v, whereas the other components do not significantly alter the wave form.

When the nozzle admittance is considered and the boundary conditions at the mixing chamber exit are imposed, the values of the modal frequencies, that is, $f_n = \mathrm{Re}(\omega)/2\pi$, and the growth constant of each mode, that is, $\alpha = -\mathrm{Im}(\omega)$, can be found by solving the corresponding boundary value problem (BVP). The BVP solution is obtained numerically by means of a procedure based on Newton's method [19]. Tentative values are assumed for the unknown head-end pressure (real and imaginary parts) and are progressively corrected to satisfy the prescribed boundary conditions. According to the present formulation, the magnitude of the acoustic pressure at the head end does not affect results and can be arbitrarily assumed.

The results presented in Figs. 4 and 5 show that the effect of the velocity-coupled response function R_v on the frequency and growth constant of the first longitudinal (L1) acoustic mode of the combustion chamber is negligible. The phase angle between pressure and velocity oscillation and the standing wave amplitude as a function of the axis abscissa are only slightly influenced by R_v. The effect of the pressure-coupled response function R_p on the growth constant

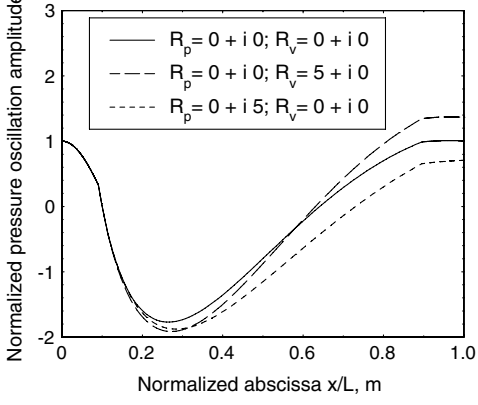

Fig. 3 Changes in standing wave amplitude due to changes in R_v and R_p.

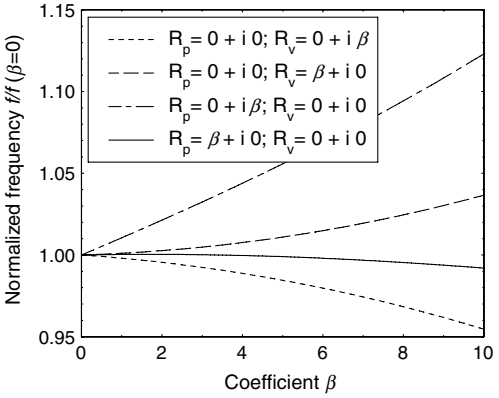

Fig. 4 Influence of the coupled response functions on the frequency of the first longitudinal mode.

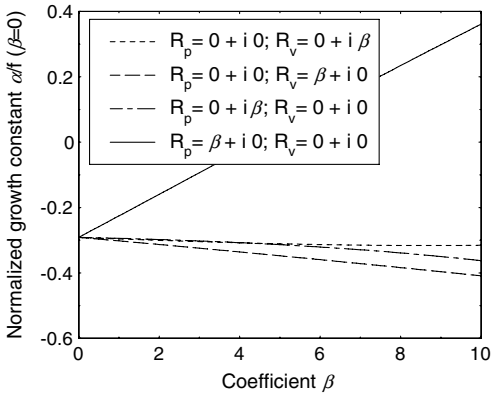

Fig. 5 Influence of the coupled response functions on the growth constant of the first longitudinal mode.

and frequency of the chamber L1 mode is instead remarkable; the imaginary part of R_p affects the standing wave amplitude and, therefore, the mode frequency, while leaving almost unchanged the mode growth constant; conversely, the real part of the pressure-coupled response function modifies the phase angle between pressure and velocity oscillation and has a large effect on the growth constant α; note that the mode becomes unstable when α becomes positive.

These results suggest that one can determine the pressure-coupled response function by measuring the growth constant and the frequency of the acoustic modes of the combustion chamber during stable operation. Conversely, if the real part of the pressure-coupled response function is known, the stability margin of the motor can be determined.

V. Nonhomogeneous Formulation

Pressure measurements performed during stable operation of a rocket motor reveal the presence of stochastic forcing noise sources that appear in the pressure auto spectrum as non-null pressure oscillations at any frequency. Thus, as far as the combustor dynamic response is concerned, the rocket chamber can be thought of as composed of an infinite series of damped oscillators driven by broadband forcing terms. If these forcing terms are given and the combustor response is measured, one can in principle derive the combustion response function at any frequency. To determine the feasibility of this approach, one should measure the nonacoustic forcing terms and then quantify the combustor dynamic sensitivity to the response function. The presence of forcing functions is taken into account assuming that the right-hand term in Eq. (21) is not null, that is,

$$\frac{\mathrm{d}}{\mathrm{d}x}\begin{bmatrix}\hat{u}\\ \hat{p}\end{bmatrix} + E(x)\begin{bmatrix}\hat{u}\\ \hat{p}\end{bmatrix} = F(x) \tag{24}$$

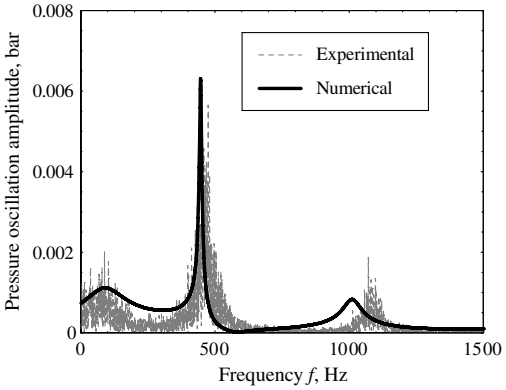

Fig. 6 Head-end pressure amplitude vs frequency with $\nu = 3.4 \cdot 10^{-4}$ ($R_v = 0 + i0$, $R_p = 5 + i4$).

The forcing term is assumed to consist of a perturbation of the solid propellant mass flow rate equal to $\nu\overline{\dot{m}}_b$, expressed as a function of a nondimensional noise level ν. Therefore,

$$F(x) = Q^{-1}(x)C(x)\nu\overline{\dot{m}}_b$$

If the nonacoustic terms are either measured or estimated, and R_p and R_v are given, then one can determine the head-end pressure for any given value of the angular frequency ω. To establish whether this approach allows for the extraction of information concerning the combustion process, a sensitivity study was performed. If the broadband noise value ν is changed, the pressure oscillation levels are roughly proportionally modified at any frequency. As far as the response functions are concerned, the effects of R_v are negligible with respect to R_p as long as pressure- and velocity-coupled response are of the same order of magnitude. The R_p imaginary part shifts the frequency of the pressure peaks. On the other hand, the real part of R_p acts on the magnitude of the pressure oscillation peaks in a peculiar way: for low values of $\mathrm{Re}(R_p)$, the low-frequency peaks are augmented, whereas larger values of $\mathrm{Re}(R_p)$ increase higher mode peaks. Figure 6 shows a comparison of the results obtained using such an approach, assuming $\nu = 3.4 \times 10^{-4}$, $R_v = 0 + i0$, and $R_p = 5 + i4$ to match the pressure oscillations that have been experimentally measured. This diagram shows that the described numerical approach can replicate the experimental results if the response functions are properly chosen. The possibility therefore exists for the deduction of combustion process behavior from dynamic pressure measurements. Actually, previous works [20,21] suggest that substantial errors may accompany system identification in the presence of noise, depending on the particular application at hand. Definite conclusions cannot be drawn yet on the basis of the present results.

In the present case, the discrepancy in the determination of the second longitudinal mode frequency may be possibly related to the interaction of this mode with vortex shedding occurring in the aft-mixing chamber, which is not accounted for in the present analysis. Vortex shedding becomes relevant when the port diameter is close to 50 mm, that is, around 15 s after ignition, as discussed at length in [2,9]. This phenomenon, in fact, may cause the shift of the second mode frequency from about 900 to 1100 Hz, as shown in Fig. 2. Other differences may be related to a possible dependence of the response functions on the frequency and to the adopted short-nozzle admittance, which is a suitable approximation when the length of the nozzle convergent section is considerably shorter than the wavelength of the oscillation and is therefore less accurate at the higher frequencies.

VI. Conclusions

A classical approach used to analyze solid rocket motor combustion instability has been successfully applied to hybrid rocket motors. A one-dimensional analysis for determining the dynamic combustion characteristics of hybrid rocket motors has been

developed. Numerical results were compared to experimental pressure measurements to gain information on the combustion process. The theoretical model accounts for mass injection from the side walls of the rocket chamber due to the combustion of the solid fuel grain and the presence of a choked nozzle. If the presence of noise sources in the control volume is neglected, then a classical acoustic problem is obtained that allows for the determination of the growth constants and frequencies of each acoustic mode. Conversely, if the growth constants and frequencies of the acoustic modes are known, the combustion response functions can be estimated at these same frequencies. Moreover, it was shown that when the presence of the nozzle was accounted for by imposing the appropriate boundary conditions, the pressure-coupled response function was solely responsible for changes of the growth constants and of the mode frequencies.

When the presence of stochastic forcing terms is accounted for in the equations, and the propellant response functions are known, the pressure fluctuations at the head end of the motor can be calculated. The noise level has a scaling effect on the pressure oscillations. Conversely, if the amplitude of pressure oscillations versus frequency is known, then the response functions can be estimated at any frequency. A preliminary sensitivity study was performed to asses the method's capabilities. Uncertainty associated with the inferred values of R_p are to be evaluated.

References

[1] Karabeyouglu, A., De Zilwa, S., Cantwell, B., and Zilliac, G., "Modeling of Hybrid Rocket Low Frequency Instabilities," *Journal of Propulsion and Power*, Vol. 21, No. 6, 2005, pp. 1107–1116. doi:10.2514/1.7792

[2] Carmicino, C., "Acoustics, Vortex Shedding and Low-Frequency Dynamics Interaction in an Unstable Hybrid Rocket," *Journal of Propulsion and Power*, Vol. 25, No. 6, 2009, pp. 1322–1335. doi:10.2514/1.42869

[3] De Zilwa, S., Zilliac, G., Reinath, M., and Karabeyoglu, A., "Time-Resolved Fuel-Grain Port Diameter Measurement in Hybrid Rocket," *Journal of Propulsion and Power*, Vol. 20, No. 4, 2004, pp. 684–689. doi:10.2514/1.2188

[4] Hessler, R. O., "Passive Linear Stability Measurements," *JANNAF Combustion Meeting*, Vol. 2, Chemical Propulsion Information Analysis Center, Columbia, MD, Oct. 1997, pp. 163–176.

[5] Culick, F. E. C., "Combustion Instabilities: Mating Dance of Chemical, Combustion, and Combustor Dynamics," AIAA Paper 2000-3178, July 2000.

[6] Hessler R. O., Glick, R. L., Bertelé, R., Cedro, D., Fiorentino, G., DeLuca, L. T., Pastrone, D., Saretto, S. R., and Vassallo, E., "Acoustic Response of a Model Rocket Chamber," *Second European Conference on Launcher Technology: Space Solid Propulsion*, Centre National d'Etudes Spatiales, Nov. 2000.

[7] Pastrone, D., Saretto, S. R., and Vassallo, E., "Acoustic Analysis of a Subscale Rocket Motor," AIAA Paper 2001-3867, July 2001.

[8] Pastrone, D., and Saretto, S. R., "An Improved Acoustic Analysis of a Subscale Rocket Motor," AIAA Paper 2003-4627, July 2003.

[9] Carmicino, C., and Russo Sorge, A., "On the Role of Vortex Shedding in Hybrid Rockets Combustion Instability," AIAA Paper 2008-5016, July 2008.

[10] Carmicino, C., and Russo Sorge, A., "Influence of a Conical Axial Injector on Hybrid Rocket Performance," *Journal of Propulsion and Power*, Vol. 22, No. 5, 2006, pp. 984–995. doi:10.2514/1.19528

[11] Carmicino, C., and Russo Sorge, A., "Performance Comparison Between Two Different Injector Configurations in a Hybrid Rocket," *Aerospace Science and Technology*, Vol. 11, No. 1, 2007, pp. 61–67. doi:10.1016/j.ast.2006.08.009

[12] Dènos, R., and Olivari, D., "Digital Data Acquisition and Processing," *Measurement Techniques in Fluid Dynamics. An Introduction*, 2nd ed., Von Karman Inst. for Fluid Dynamics, Rhode-St-Genèse, Belgium, 2001.

[13] Qian, S., and Chen, D., *Joint Time-Frequency Analysis—Methods and Applications*, Prentice–Hall, Upper Saddle River, NJ, 1996.

[14] Micci, M. M., Caveny, L. H., and Sirignano, W. A., "Linear Analysis of Forced Longitudinal Waves in Rocket Motor Chambers," *AIAA Journal*, Vol. 19, No. 2, 1981, pp. 198–204. doi:10.2514/3.7757

[15] Culick, F. E. C., "Stability of Longitudinal Oscillations with Pressure and Velocity Coupling in a Solid Propellant Rocket Motor," *Combustion Science and Technology*, Vol. 2, 1970, pp. 179–201. doi:10.1080/00102207008952247

[16] Levine, J. N., and Baum, J. D., "A Numerical Study of Nonlinear Instability Phenomena in Solid Rocket Motors," *AIAA Journal*, Vol. 21, No. 4, 1983, pp. 557–564. doi:10.2514/3.8113

[17] Bussi, G., Colasurdo, G., and Pastrone, D., "Nozzle Effects on Linear Stability Behaviour of Combustors," *11th International Symposium on Air Breathing Engines*, Vol. 1, AIAA, Washington, DC, Sept. 1993, pp. 486–492; also AIAA Paper 93-7044.

[18] Carmicino, C., and Russo Sorge, A., "Role of Injection in Hybrid Rockets Regression Rate Behavior," *Journal of Propulsion and Power*, Vol. 21, No. 4, 2005, pp. 606–612. doi:10.2514/1.9945

[19] Colasurdo, G., and Pastrone, D., "Indirect Optimization Method for Impulsive Transfer," AIAA Paper 1994-3762, Aug. 1994.

[20] Seywert, C., "Combustion Instabilities: Issues in Modeling and Control," Ph.D. Thesis, Jet Propulsion Lab. California Inst. of Technology, Pasadena, CA, 2001.

[21] Seywert, C., and Culick, F. E. C., "Comparison of Different Approaches for the Approximate Analysis of Combustion Instabilities," *34th JANNAF Combustion Meeting*, Vol. 1, Chemical Propulsion Information Analysis Center, Columbia, MD, 1998, pp. 463–469.

T. Lieuwen
Associate Editor